AIAA JOURNAL
Vol. 39, No. 6, June 2001

# Electron-Beam-Generated Plasmas in Hypersonic Magnetohydrodynamic Channels

Sergey O. Macheret,* Mikhail N. Shneider,† and Richard B. Miles‡
*Princeton University, Princeton, New Jersey 08544-5263*
and
Ronald J. Lipinski§
*Sandia National Laboratories, Albuquerque, New Mexico 87185*

**A novel concept is analyzed of hypersonic cold-air magnetohydrodynamic (MHD) power generators and accelerators with ionization by electron beams. Ionization processes are considered in detail. Strong coupling between hypersonic boundary layers and electrode sheaths is demonstrated, and anode voltage fall in hypersonic MHD channels is shown to be very high. A potential anode sheath instability and ways to suppress it are discussed. Electron beams are shown to be capable of generating an adequate conductivity in cold air, while allowing full control and stable operation of MHD channels. Example calculations of hypersonic accelerator and power generator performance appear to be promising.**

## I. Introduction

OVER the past several years, new applications of magnetohydrodynamic (MHD) technology to hypersonics have been proposed. One concept, called AJAX, was proposed in Russia about 10 years ago.[1,2] A key element of AJAX is a MHD power generator at the inlet of the airbreathing hypersonic engine. The MHD device would reduce the total enthalpy of the flow, which could allow the engine to operate in subsonic or low-supersonic regime in a hypersonic flight. The generated electricity could be used to power various electromagnetic devices onboard or to provide a MHD acceleration of the engine exhaust flow (the so-called MHD bypass).

Another proposal is a MHD acceleration of hypersonic flow that would allow building a long run time, high dynamic pressure, medium- or large-scale hypersonic wind tunnel.[3,4] Currently under development as a part of the MARIAH II project, this concept relies on an ultrahigh-pressure (10,000–20,000 atm), low-temperature (about 1000 K) plenum, followed by laser or electron-beam energy addition to dense air as it expands in the supersonic nozzle and subsequent augmentation of total enthalpy in a hypersonic MHD accelerator channel.

Potentially, both novel MHD applications, power extraction and flow acceleration, could revolutionize high-speed flight. However, there are substantial scientific and engineering challenges in the development of these concepts. The challenges result from the range of conditions and parameters dictated by the applications.

In both AJAX and MARIAH II, air would enter the MHD channel with a static pressure of about 0.1 atm, temperature of a few hundred Kelvin (in AJAX, the static temperature could reach about 1000 K at the channel exit), and velocity of 2000–4000 m/s. This range of conditions drastically differs from that in conventional MHD channels. Those channels use high-temperature (above 2500 K) gas seeded with alkali metals to produce an adequate ionization. This traditional method of sustaining electrical conductivity would not work for AJAX power generators and MARIAH II accelerators. At hypersonic speeds, Mach 8 and above, mixing of the injected seed with the flow is very problematic. More important, at temperatures of 1000 K and lower, thermal ionization of even cesium is far below that required for MHD operation. Additionally, thermal ionization in hot hypersonic boundary layers would be much higher than in the core flow, resulting in short circuiting through the boundary layer.

Cold hypersonic MHD channels would, therefore, have to rely on a nonthermal ionization mechanism. Of course, ionization is not in equilibrium in all glow discharges. There, electrons receive energy from an electric field, and, because of slow electron–molecule energy exchange due to large mass difference, high electron temperature can be sustained. With mean electron energy of at least a few electronvolts, there is a substantial fraction of high-energy electrons capable of ionizing molecules in collisions. However, there are major obstacles to using this ionization mechanism in MHD channels. First, to minimize joule heating and entropy increase in the channel, an effective electric field has to be very low,[3,4] resulting in electron temperatures below 1 eV. Such electric fields and electron temperatures would not be enough for the needed ionization of air. Introducing a seed with low ionization energy, and thus combining seeding with nonequilibrium ionization, may seem attractive. Nevertheless, this approach is very problematic because of the mixing problem and short circuiting through the boundary layer as described in the preceding paragraph.

Another problem associated with nonequilibrium ionization is an instability that tends to break an initially uniform cold diffuse plasma into narrow hot arcs. Indeed, if a fluctuation locally increases temperature and reduces density, an increased electron mean free path would allow electrons to gain more energy from the electric field, resulting in higher local electron temperature. This would locally enhance ionization and joule heating, increasing temperature even further, etc. High gas density and strong magnetic fields both tend to restrict electron mobility and heat conduction, preventing local fluctuations of temperature and electron density from dissipating rapidly, thus lowering the instability threshold.

Thus, devising an effective and stable method of generating an adequate nonthermal ionization is the first-order problem in developing hypersonic MHD devices. In this paper, we present and analyze such a method: injecting high-energy electron beams into the channel along magnetic field lines. In Sec. II, the method and its potential advantages are described. In Sec. III, modeling of ionization profiles created by electron beams is discussed, focusing on ionization uniformity and its effects on supersonic flow. In Sec. IV, we discuss phenomena occurring near channel walls and electrodes. In Sec. V, simplified models of charge kinetics and vibrational relaxation relevant to hypersonic MHD plasmas are described, and sample results of modeling MHD accelerators and power generators

Presented as Paper 99-3635 at the 33rd Thermophysics Conference, Norfolk, VA, 28 June–1 July 1999; received 15 March 2000; revision received 8 December 2000; accepted for publication 8 December 2000. Copyright © 2001 by the American Institute of Aeronautics and Astronautics, Inc. All rights reserved.

*Research Scientist, Department of Mechanical and Aerospace Engineering, D-414 Engineering Quadrangle. Associate Fellow AIAA.
†Research Staff Member, Department of Mechanical and Aerospace Engineering, D-414 Engineering Quadrangle. Member AIAA.
‡Professor, Department of Mechanical and Aerospace Engineering, D-414 Engineering Quadrangle. Fellow AIAA.
§Distinguished Member of the Technical Staff, MS-1146, P.O. Box 5800. Member AIAA.

with electron-beam ionization are shown. Finally, in Sec. VI, a summary of findings and outline of future work are given.

## II. Electron-Beam Ionization in MHD Channels: Qualitative Analysis and Potential Advantages

As discussed, the hypersonic MHD channels would operate at low temperatures and low values of electric field. These conditions, together with the need to avoid short circuiting through hot, highly conductive boundary layers, and with the great difficulties in mixing injected seed with hypersonic flow, preclude the use of both thermal and nonequilibrium self-sustained ionization. Thus, the only way to sustain an adequate conductivity is to use an external ionizer.

High-energy electron beams are, of course, the most efficient ionization sources. For the most efficient transfer of the required ionization energy to an outer-shell electron, the mass of the incident particle should be equal to the electron mass. Therefore, photons and heavy particles (atoms, ions) are much less efficient. Additionally, in a plasma, such as that in glow discharges, where mean electron energy is a few electronvolts, only a small fraction of the electrons (the high-energy tail) would actually do the ionization, while most of the energy received from the electric field is spent on excitation of molecular and atomic states and on heating. In contrast, high-energy beam electrons would collisionally ionize atoms and molecules with very high probability, and secondary electrons would cause additional ionization. Thus, a cascade of electrons is generated as the beam slows down. The net effect is approximately one ionized molecule or atom for every 35 eV lost by the beam. This ionization cost is only two to three times greater than the ionization energy of air molecules.

The basic configuration of a Faraday MHD channel with electron-beam ionization is shown in Figs. 1 and 2. An array of individually ballasted segmented electrodes creates a transverse electric field and generates an electric current. The magnetic field, orthogonal to both the electric field and the flow direction, produces the accelerating or decelerating $\boldsymbol{j} \times \boldsymbol{B}$ force (in Figs. 1 and 2, the accelerator case is shown). Total flow enthalpy is affected not only by the $\boldsymbol{j} \times \boldsymbol{B}$ force, but also by the inevitable joule heating and by the energy input from the ionizating beams. The beams, as shown in Figs. 1 and 2, have to be injected along magnetic field lines because the electrons tend to spiral around the field lines and calculations show that the Larmor radius is less than a millimeter under typical conditions of AJAX and MARIAH II channels.

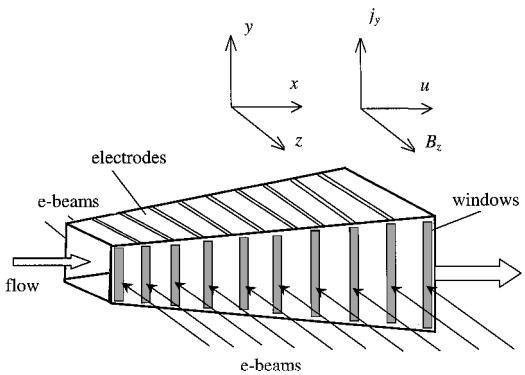


**Fig. 1 Schematic of an MHD channel with electron-beam ionization.**

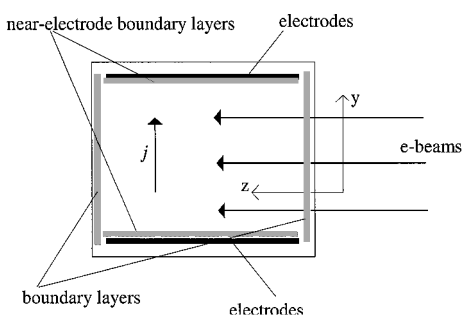


**Fig. 2 Schematic of an MHD channel with electron-beam ionization: side view.**

To impart or extract an enthalpy of a few megajoules per kilogram to/from airflow at densities on the order of 0.1-atm density, over a reasonable length, 1–4 m, an electron number density at least on the order of $10^{12}$–$10^{13}$ cm$^{-3}$ is required.[3,4] Estimates performed in Refs. 3 and 4 indicate that this electron number density could be sustained by an array of electron beams with energy of 10–50 keV and beam current density of between 1 and 100 mA/cm$^2$.

As a practical matter, it would be very hard if not impossible to have electron beams fill out the entire sidewall of the channel more or less uniformly. Indeed, the beams would be generated in vacuum and would have to be injected into the channel through some foils or windows. The windows or foils would be heated by the beams passing through and also would have to be of sufficient mechanical strength. If the beam current density is on the order of 1 mA/cm$^2$ or less, thin metallic foils with passive cooling should suffice.[5] For higher beam current densities, either active cooling or the new technology of so-called plasma windows or ports[6,7] would have to be utilized. In any case, electron beams will be passed through only a part of the sidewall, and Fig. 1 shows the pass-through foils or windows as a periodic array of strips.

The rate of energy loss by the beam electrons is fairly independent of energy if the electron energy is greater than a few hundred kiloelectron volts (Refs. 5 and 8). However, in the 30-keV range, the energy loss per unit length traversed increases strongly as the electron energy decreases. Thus, the energy deposition per unit length by the beam is not uniform across the MHD channel. In addition, the electrons tend to follow the magnetic field across the channel because any attempt to travel perpendicular to the field lines results in a helical path due to the Lorentz force.

Modeling of electron-beam-generated ionization profile across the channel will be addressed in the next section. To conclude this section, we list several advantages of the ionization by electron beams.

1) Electron beams represent the most efficient way of ionizing cold gases. Even at low temperatures and low electric field, an adequate electrical conductivity for MHD operation can be created with reasonable beam energy and current.

2) Because for high electron energies ionization cross sections increase when the incident electron energy decreases, beams injected from the sidewall would generate higher ionization inside the channel than near the wall. Thus, the problem of short circuiting through the hot, highly conductive boundary layer, severely limiting performance of conventional MHD devices, can be minimized in devices with electron-beam ionization.

3) Collisional plasmas with externally sustained ionization are inherently more stable than those of self-sustained nonequilibrium discharges. Indeed, ionization generated by electron beams is essentially decoupled from both temperature and electric field. A local positive fluctuation in temperature that would have led to arcing instability in self-sustained discharges (see preceding section) would result in reduced ionization by electron beams and reduced local heating, stabilizing the plasma. Moreover, conventional MHD devices cannot operate at high values of Hall parameter. (A Hall parameter is the ratio of the electron cyclotron frequency to the electron, heavy particle collision frequency.) This is due to reduced electron mobility across the magnetic field, which prevents electron density fluctuations from dissipating, leading to instability, similar to the ionization–thermal instability at high pressures. Although, to our knowledge, stability of MHD plasmas with external ionization has not been studied, it is conceivable that having an ionization source independent of temperature and local electron density could break the instability loop. Note that collisionless plasma instabilities such as the beam–plasma instability that would transfer energy of beam electrons into Langmuir oscillations would not be important at the relatively high gas densities and low beam currents considered in this paper.

## III. Electron-Beam-Generated Ionization Profiles

Ionization profiles generated by electron beams can be computed by the CYLTRAN code developed at Sandia National Laboratories

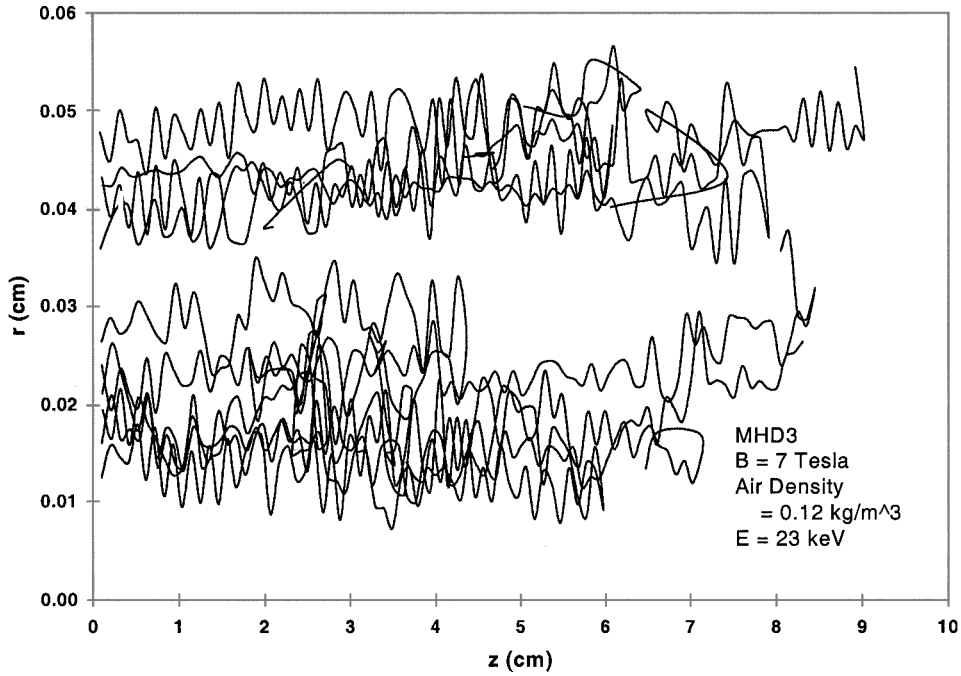


**Fig. 3 Trajectories of 10 primary electrons for a 23-keV electron beam injected from the left side of the graph at $z = 0$ cm.**

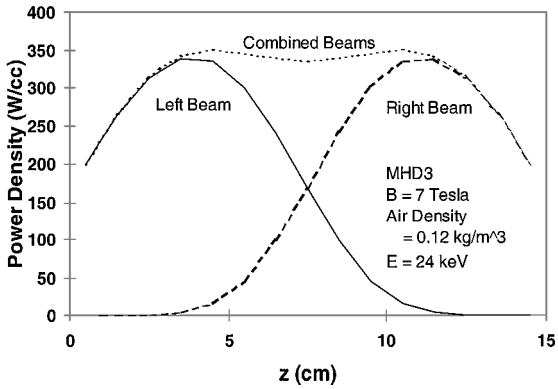


**Fig. 4 Power deposition for a uniform electron-beam injected from the left (——) and right (- - - -) and the total power deposition from the two beams ( · · · ·).**

as a part of the Integrated Tiger Series (ITS) codes.[9] CYLTRAN is a Monte Carlo type code computing many individual trajectories and incorporating elastic and inelastic scattering. The code was exercised by one of the authors (Lipinski) for typical conditions expected in hypersonic MHD channels. Figure 3 shows the individual electron trajectories for separate 23-keV electrons injected from the left side of the graph at $z = 0$. Note how the 7-T field overcomes the scattering from collisions with the air and keeps the electrons traveling straight across the channel. Note also how the electrons come to rest at different final locations. This effect is called straggling.

Figure 4 shows the energy deposition rate (in watts per cubic centimeter) for a uniform beam (which in this case means it is uniform in the $x$ and $y$ direction for at least several millimeters because that is the zone that the magnetic field confines the beam to). The solid line shows the deposition rate for a beam injected from the left side of the graph. Note how the deposition rate increases as the beam progresses and loses energy. (Lower-energy electrons deposit energy more rapidly.) However, the total deposition rate then starts to fall off due to straggling because some of the electrons come to a stop before others.

The power deposition profile will match the induced conductivity profile, and so we really would prefer a more uniform deposition than is shown in Fig. 4 by the solid line. A solution is to have another beam injected from the other side in the opposite direction. This is shown in Fig. 4 as a dashed line. The total deposition will be the sum of the two and is shown as a dotted line. It is fairly uniform if the initial beam energy for both beams is 23 keV.

The CYLTRAN trajectory code is capable of predicting the beam energy deposition and ionization rate profiles across the channel, provided that the density profile is known. However, to build a comprehensive computational model, the beam propagation code has to be coupled with two- or three-dimensional viscous gasdynamics, electrodynamics, and ionization–recombination kinetics. Monte Carlo trajectory codes are very computationally intensive, and their inclusion into full models could be done only at the expense of oversimplified kinetics and MHD.

An alternative approach is to use differential equations in the so-called forward–backward approximation,[4] suggested in Ref. 10 and, independently, in Ref. 11. This approach is essentially quasi one dimensional, and it can be used in our case because (as seen in Fig. 3) given that the Larmor radius of the beam electrons in a magnetic field of several tesla is less than a millimeter, the beams spiral around the magnetic field lines virtually without lateral scattering.

Kinetic equations for beam electrons in the forward–backward approximation assume that all electrons move along the $z$ axis and that they scatter in elastic collisions with molecules either forward or, with a probability $\xi$, backward. In inelastic processes, such as excitation and ionization of molecules, electrons lose their energy, but are assumed not to deviate from the direction of their motion.

At steady state, the two unidirectional (parallel and antiparallel to $z$ axis) spectral fluxes, that is, fluxes of beam electrons having energy between $\varepsilon$ and $(\varepsilon + d\varepsilon)$, assuming no electric field component in $z$ direction, can be found from[4,10]

$$\frac{\partial \Gamma_1}{\partial z} = \xi \frac{\Gamma_2 - \Gamma_1}{l_m(\varepsilon)} + Q(\Gamma_1), \qquad \frac{\partial \Gamma_2}{\partial z} = \xi \frac{\Gamma_1 - \Gamma_2}{l_m(\varepsilon)} + Q(\Gamma_2) \quad (1)$$

where $Q$ are inelastic electron collision terms and $l_m(\varepsilon)$ is the electron–molecule momentum-transfer mean free path determined by the transport cross section $\sigma_m(\varepsilon)$. For gas mixtures,

$$\frac{1}{l_m(\varepsilon)} = \sum_k N_k \sigma_{m,k}(\varepsilon) \quad (2)$$

where $N_k$ are number densities of the components of the mixture.

Excitation of the $n$th quantum state of a molecule of the $k$th component, requiring electron energy $I_n^k$, and electron-impact

ionization, requiring, in the first approximation, energy equal to the ionization potential $I_i^k$, lead to inelastic collision terms $Q$:

$$Q_k(\Gamma_{1,2}) = -\sum_{n,k} N_k \Gamma_{1,2}(z, \varepsilon)\sigma_n^k(\varepsilon) + \sum_{n,k} N_k \Gamma_{1,2}\left(z, \varepsilon + I_n^k\right)\sigma_n^k\left(\varepsilon + I_n^k\right) \quad (3)$$

where $\sigma_n^k(\varepsilon)$ are excitation and ionization (lower index $i$) cross sections, and the 1 and 2 subscripts imply either the parallel or antiparallel to the beam component. The local ionization rate is the number of ionization events in 1 cm$^3$/1 s at a given location $z$:

$$q(z) = \sum_k N_k \int_{I_i^k}^{\infty} (\Gamma_1 + \Gamma_2)\sigma_i^k(\varepsilon)\,\mathrm{d}\varepsilon \quad (4)$$

One of the well-known parameters of electron-beam interaction with gases is the so-called ionization cost $W_i^k$, that is, the mean energy of production of an electron–ion pair in beam electron collisions with molecules of the $k$th component. At primary electron energies above a few hundred electronvolts, $W_i^k$ is virtually independent of the beam energy spectrum and is determined by the gas composition only. For example, in air, pure nitrogen, and oxygen, $W_i = 34$, 35, and 30.9 eV, respectively.[4,5,8] Therefore, in the inelastic collision integral $Q$ for fast electrons, the term corresponding to the source of electrons of energy $\varepsilon$ due to ionization can be written as

$$\sum_k N_k \Gamma_{1,2}\left(z, \varepsilon + W_i^k\right)\sigma_i^k\left(\varepsilon + W_i^k\right), \qquad \varepsilon + W_i^k \le \varepsilon_b \quad (5)$$

where $\varepsilon_b$ is the beam electron energy.

Boundary conditions and the procedure of solving kinetic equation in the forward–backward approximation are discussed in detail in Ref. 10.

Despite being significantly simpler than Monte Carlo methods, and almost as accurate,[10] self-consistent computations employing forward–backward approximation are still quite cumbersome due to the need to iterate at each time step. The problem is simplified if the kinetic equation is solved in the forward approximation[4,10] considering only inelastic electron–molecule collisions that are assumed not to change the direction of electron motion. This approximation is justified in our case because, for the main, ionizing part of the energy spectrum of the beam, inelastic cross sections considerably exceed the momentum-transfer cross section $\sigma_n^k(\varepsilon) \gg \sigma_m(\varepsilon)$, when $\varepsilon > 500$ eV.

As demonstrated in Refs. 4 and 10, the forward approximation gives a good accuracy compared with the full forward–backward method, and both of them agree reasonably well with Monte Carlo modeling. Computations of ionization profiles across an air channel using the forward approximation were discussed in detail in Refs. 4 and 12. In Ref. 12, effects of nonuniform ionization profiles were explored by solving two-dimensional Navier–Stokes equations coupled with electron-beam propagation across the channel and beam-generated ionization profiles in a constant-area duct.

## IV. Electrode Sheaths and Boundary Layers in Hypersonic MHD Channels

### A. Qualitative Analysis

Understanding near-electrode space-charge sheaths and fluid boundary layers in hypersonic MHD channels is critical because of a strong coupling between charge particle kinetics, electromagnetics, and fluid mechanics. Here, we only present a qualitative analysis, illustrated by a few sample calculations. Note that turbulent boundary-layer calculations in Ref. 13 and in the present paper used the turbulence model described in Refs. 14 and 15. Turbulent transport was accounted for by an effective eddy viscosity, using the algebraic Prandtl–Boussinesq model (see Refs. 14 and 15).

Modeling of plasma flows in MHD power generators and accelerators is usually done within the framework of single-fluid MHD. For processes inside the plasma, far from the walls and electrodes, this approximation is quite justified. However, because a strong transverse electric current has to be sustained in the channel to give rise to accelerating or decelerating ponderomotive (or ampere) forces, pronounced cathode and anode charge sheaths are necessarily formed through which the current has to flow. In a strong transverse magnetic field, electron mobility is reduced, which can dramatically alter characteristics of the near-electrode sheaths, especially those of the anode sheath. The thickness of the sheaths can be comparable with that of the hypersonic fluid and thermal boundary layers. This can result in a strong coupling between the charge sheaths and fluid boundary layers. For example, characteristics of a charge sheath would be affected by the reduced density, high temperature, and turbulence in the hypersonic boundary layer, whereas the ponderomotive force could significantly increase or decrease the effective viscosity, thus changing the boundary layer.

Two-dimensional modeling of ionized gas flow in an MHD accelerator depends substantially on the choice of the coordinate plane. In the $(x, z)$ or $(u, B_z)$ plane, there is no electric current, and the plasma is quasi neutral everywhere except in near-wall regions with the thickness of the order of the debye length. The debye length is negligibly small in comparison with the boundary-layer thickness $\delta$, and the voltage fall across the near-wall regions, $\Delta V_z \sim T_e$, can be neglected. Therefore, the flow in this plane can be treated with single-fluid MHD.

Much more complex is the flow in the $(x, y)$ or $(u, j_y)$ plane, where electric current $j_y$ gives rise to the ponderomotive force directed along $x$. Near the walls that are also electrodes, charge separation occurs forming the anode and cathode sheaths. It is well known that the anode voltage fall $V_a$ and the anode sheath thickness $d_a$ are negligible compared with the respective cathode-sheath values $V_c$ and $d_c$ (Ref. 16). The dramatic difference between the anode and cathode sheaths stems from the strong difference between electron and ion mobilities under normal conditions, $\mu_e/\mu_+ \sim 10^2$. However, in our case, electrode sheaths are immersed into hot and rarefied hypersonic boundary layers. Additionally, and very importantly, electric current in the sheaths has to flow across a strong magnetic field that substantially reduces electron mobility. Thus, one could expect boundary layers and electrode sheaths to be very different from those in conventional non-self-sustained transverse discharges.

Let us find out how the presence of a strong magnetic field $B_z$ and the nonuniform density profile in the boundary layer, $N(x, y)$, affects structure and parameters of cathode and anode sheaths in a hypersonic flow transverse discharge supported by electron beams.

A key problem in modeling electrode sheaths that are also boundary layers is to determine what heating mechanism, viscous dissipation or joule heating, is dominant. Viscous dissipation rate in the boundary layer is

$$W_\eta(y) = \frac{\partial}{\partial y}\left((\eta + \eta_T)u\frac{\partial u}{\partial y}\right) \quad (6)$$

An estimate of this dissipation rate for a turbulent boundary layers is $W_\eta \approx \bar{\eta}_T u_{\mathrm{ext}}^2/\delta^2$, where $\bar{\eta}_T$ is the effective turbulent dynamic viscosity coefficient, averaged over the boundary layer. According to the algebraic Prandtl–Boussinesq model in a Clauser approximation, modified by Cebeci and Smith,[14]

$$\bar{\eta}_T = \tilde{\alpha}\rho u_{\mathrm{ext}}\left|\int_0^{\infty}\left(1 - \frac{u}{u_{\mathrm{ext}}}\right)\mathrm{d}y\right| \approx \tilde{\alpha}\rho u_{\mathrm{ext}}\delta$$

where $u_{\mathrm{ext}}$ is the flow velocity at the edge of the boundary layer and $\tilde{\alpha} \approx 0.0168$. For typical conditions of interest in this paper, $p = 0.1$ atm, the ratio of the peak temperature in the boundary layer to that in the core flow $T_{\max}/T_0 \sim 10$, boundary-layer thickness $\delta \approx 10^{-3}$ m, and the flow velocity $u_{\mathrm{ext}} = 3500$ m/s, the effective viscosity is $\bar{\eta}_T \approx 1.76 \times 10^{-3}$ kg/(m · s), and the rate of viscous dissipation is $W_\eta \approx 2.25 \times 10^{10}$ W/m$^3$.

When evaluating joule heating in the boundary layer, one has to bear in mind that, although in Faraday-type MHD devices there is no longitudinal current ($j_x = 0$) in the core flow, the longitudinal current in the boundary layer can be quite large. Therefore, the joule dissipation rate can be calculated as

$$W_J = \left(j_x^2 + j_y^2\right)/\sigma \quad (7)$$

where current density and electric field components are[16–19]

$$j_x = \frac{\sigma\left(E_x^* - \Omega E_y^*\right)}{1+\Omega^2}, \qquad j_y = \frac{\sigma\left(E_y^* + \Omega E_x^*\right)}{1+\Omega^2} \tag{8}$$

$$E_x^* = \Omega(E_y - uB)_{|\text{ext}} = \text{const}, \qquad E_y^* = E_y - uB \tag{9}$$

where $\sigma$ is the electrical conductivity and $\Omega$ is the Hall parameter. In the core flow of Faraday-type MHD devices, where $j_x = 0$, joule heating rate is $W_J = j_y^2/\sigma = j_y E_y^* = (k-1)^2 \sigma u^2 B^2$, where $k$ is the loading parameter. At the transverse current density $j_y = 5 \times 10^3$ A/m$^2$, loading parameter $k = 1.1$, flow velocity $u = 3500$ m/s, and magnetic field $B = 20$ T, the joule heating in the core flow is $W_{J|\text{ext}} \approx 3.5 \times 10^6$ W/m$^3$, which is much lower than the viscous dissipation rate per unit volume in the boundary layer.

However, in electrode sheaths immersed into heated and rarefied boundary layers, joule heating greatly increases as compared with that in the core flow. First, due to charge separation and reduced mobility of charge carriers, the transverse electric field may greatly exceed that in the core flow. Second, because of the low gas velocity, the longitudinal Hall current becomes essential[19]: $j_x \approx \Omega(y) j_y$. In the general case, term (13) should be added into the energy equation of boundary-layer theory, as was done by Kerrebrock.[20] Development of a self-consistent theory of boundary layers and electrode sheaths is a very complex problem. In the first approximation, we can uncouple electrode sheaths from the boundary layers and calculate the sheath structure as an overlay on independently computed boundary layers. If then it turns out that joule heating in the sheath is small compared with the viscous dissipation rate, such an uncoupled analysis would be complete. If, however, the joule heating is stronger than the viscous dissipation, this would indicate a need for a fully coupled computation and also point to a possible instability.

### B. Charge Particle Kinetics

The transverse non-self-sustained discharge in gas flow was modeled with a standard set of continuity equations for electron and ion number densities, $n_e$ and $n_+$, plus the Poisson equation for the electric field $\boldsymbol{E}$:

$$\frac{\partial n_+}{\partial t} + \operatorname{div} \boldsymbol{\Gamma}_+ = q + \alpha\left(\frac{E_{\text{eff}}}{N}\right)\left|\boldsymbol{\Gamma}_{e,\text{dr}}\right| - \beta n_+ n_e \tag{10}$$

$$\frac{\partial n_e}{\partial t} + \operatorname{div} \boldsymbol{\Gamma}_e = q + \alpha\left(\frac{E_{\text{eff}}}{N}\right)\left|\boldsymbol{\Gamma}_{e,\text{dr}}\right| - \beta n_+ n_e \tag{11}$$

$$\operatorname{div} \boldsymbol{E} = \frac{e}{\varepsilon_0}(n_+ - n_e) \tag{12}$$

where $\boldsymbol{\Gamma}_e = n_e \boldsymbol{v}_e$ and $\boldsymbol{\Gamma}_+ = n_+ \boldsymbol{v}_+$ are the charged particle fluxes, $\boldsymbol{\Gamma}_{e,\text{dr}}$ is the ionizing drift component of the electron flux (that is, the flux without the convective component that does not contribute to electric current density), $q(y) = q_{\text{ext}} N(y)/N_{\text{ext}}$ approximates the rate of ionization produced by the electron beam, and gas density $N(y) \propto T^{-1}(y)$ is considered to be determined by the solution of the boundary-layer problem. In the continuity equations (10) and (11), account is also taken of electric-field-induced ionization, which may turn out to be substantial in those regions where the field is strong and the gas is rarefied. For the field-induced ionization, we use the conventional local Townsend approximation $\alpha = \alpha(E_{\text{eff}}/N)$ (see Ref. 16), with the effective electric field in the case of crossed electric and magnetic field[17]:

$$E_{\text{eff}} = \left[\frac{E_x^2 + (E_y - uB_z)^2}{1+\Omega^2}\right]^{\frac{1}{2}} \tag{13}$$

where $\Omega = eB_z/m\nu_m \equiv \omega_c/\nu_m$ is the Hall parameter for electrons and $\omega_c = eB_z/m$ and $\nu_m$ are the electron cyclotron and collision frequencies. In what is to follow, we will use similar parameters for ions: $\Omega_+ = eB_z/M\nu_{\text{in}} \equiv \omega_c^+/\nu_{\text{in}}$, where $\nu_{\text{in}}$ is the ion–neutral collision frequency. If the strongest variation of charged particle fluxes in near-electrode sheaths occurs in the direction normal to the electrodes, an approximation $\operatorname{div} \boldsymbol{\Gamma} \approx \partial \Gamma_y/\partial y$ can be used in Eqs. (10) and (11).

The boundary conditions at the electrode surface are, for the cathode,

$$\boldsymbol{\Gamma}_e = -\gamma \boldsymbol{\Gamma}_+ \tag{14}$$

where $\gamma$ is the effective coefficient of secondary emission, and, at the anode,

$$\boldsymbol{\Gamma}_+ = 0 \tag{15}$$

Quasi-neutral plasma density at the outer edge of the boundary-layer ($y = y_{\max}$) was determined by the ionization rate of $q_{\text{ext}} = 10^{20}$ cm$^{-3}$ s$^{-1}$, which is close to the average ionization rate produced by the beam with the current density $j_b = 0.1$ A/cm$^2$ and initial electron energy $\varepsilon_b = 19.5$ keV, and electron–ion dissociative recombination with the rate coefficient $\beta = 2 \times 10^{-7}$ cm$^{-3}$ s$^{-1}$, that is, $n = n_{e,\text{ext}} \approx n_{+,\text{ext}} = \sqrt{(q_{\text{ext}}/\beta)}$.

Note that in the present paper we seek solution of the Poisson equation only along the transverse coordinate $y$. The longitudinal electric field is defined by the following. As is well known, for optimal performance of an MHD accelerator, the Hall current should be compensated, that is, $j_x = 0$ (Refs. 18 and 19). This compensation is possible when the longitudinal electric field in the plasma is

$$E_x = \Omega(E_y - uB_z) \tag{16}$$

On the other hand, for the conditions considered, the electric field is potential, and the longitudinal and transverse electric field components are related by the Maxwell equation

$$\nabla \times \boldsymbol{E} = 0 \qquad \text{or} \qquad \frac{\partial E_x}{\partial y} - \frac{\partial E_y}{\partial x} = 0 \tag{17}$$

From Eq. (17), $E_x$ is constant with $y$ only when the transverse field $E_y$ is constant along the flow. Ohm's law for the current density $j_y$ then dictates that, at $E_{y,\text{ext}} = \text{const}$, a condition $\mathrm{d}(j_y/\sigma_{\text{ext}})/\mathrm{d}u_{\text{ext}} = -B_z$ should be satisfied, in a uniform magnetic field.[13] Thus, at quasi-constant conductivity, $\sigma_{\text{ext}} \approx \text{const}$, the current density $j_y$ has to vary along the channel. In the computations, we assumed $E_x = \Omega(E_y - uB_z)_{|\text{ext}} = \text{const}$. We realize that this condition represents a rather crude approximation for the boundary layer and, certainly, for near-electrode sheaths. More realistic calculation of $E_x$ would be possible only within a full two- or three-dimensional problem, which is outside the scope of the present paper.

### C. Examples of Electrode-Sheath Structure

Computations of anode-sheath structures are shown in Figs. 5 and 6. In the computations, we assumed for simplicity that the ionizing electron beams fill out the entire side wall of the channel. Boundary layers were computed at 50 cm downstream from the MHD accelerator entrance, with the core flow velocity of 3500 m/s and static pressure $p = 0.1$ atm. Anode-sheath structure was then computed as an overlay on the boundary layer, for the current density $j_y = 0.5$ A/cm$^2$ and magnetic field of $B = B_z = 20$ T. Two ionization mechanisms were included in the calculations: ionization by the injected electron beams, as in the core flow, and ionization by plasma electrons accelerated in strong near-anode electric field. The ionization rate due to plasma electrons was calculated as

$$q_1(y) = \alpha(E_{\text{eff}}/N)\left(j_x^2 + j_y^2\right)^{\frac{1}{2}}\Big/ e \tag{18}$$

where, as before, $\alpha$ is Townsend ionization coefficient and $E_{\text{eff}}$ is determined by Eq. (13). The contribution of this ionization mechanism was found to be significant, due to both high values of $E_{\text{eff}}/N$ and strong Hall current $j_x$ in the sheath.

The computed cases 1, 2, and 3 in Figs. 5 and 6 correspond to different assumptions regarding the rate of beam-induced ionization. If the current density of the beams near the anode is the same as that in the core flow (case 1), then the beam-induced ionization rate $q$ would be proportional to the gas number density $N$: $q = q_{\text{ext}} N/N_{\text{ext}}$, where $N_{\text{ext}}$ is the gas number density in the core flow, which translates to a very low ionization rate in the hot, rarefied boundary layer. Because of the need to sustain electric current, combined with the reduced electron mobility across the strong magnetic field, this results in

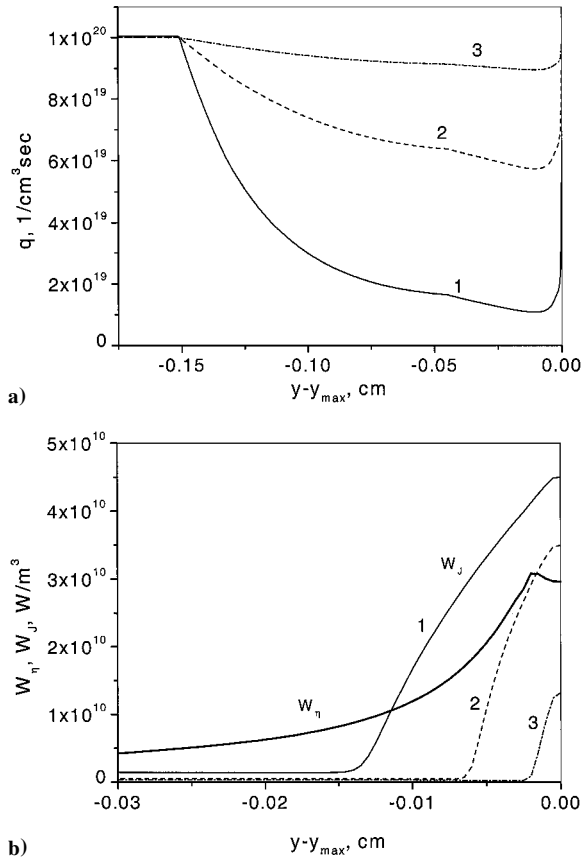


**Fig. 5 Computations of anode-sheath structures; curves 1, 2, and 3 correspond to different assumptions about the rate of beam-induced ionization: case 1 $q = q_0 N(y)/N_{\text{ext}}$, case 2 $q = q_0[N(y)/N_{\text{ext}}]^{0.25}$, and case 3 $q = q_0[N(y)/N_{\text{ext}}]^{0.05}$ and computed anode voltage falls in the three cases are $V_{a1} = 695$ V, $V_{a2} = 260$ V, and $V_{a3} = 35$ V: a) Ionization rate $q$ and b) rates of viscous ($W_\eta$) and joule ($W_J$) dissipation in the anode sheath as functions of distance to the anode.**

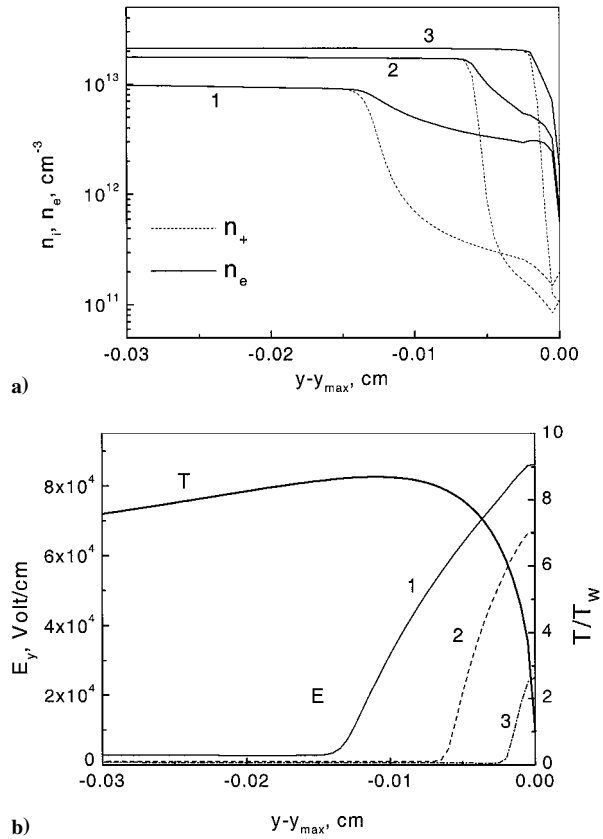


**Fig. 6 For parameters of Fig. 5: a) electron and ion number densities and b) transverse electric field $E_y$ and the ratio of gas temperature to the wall temperature $T/T_W$ as functions of distance to the anode.**

a wide anode sheath with high voltage fall and transverse electric field (Fig. 6, curves 1). The reduced conductivity and the strong Hall current $j_x$ in the sheath result in a joule heating rate that somewhat exceeds the rate of viscous dissipation (Fig. 5, curves 1). That $W_J$ exceeds $W_\eta$ by no more than a factor of 2 is because in this hypersonic regime, with core flow velocities about 3500 m/s, viscous dissipation rate $W_\eta$ in the boundary layer is very high. Because $W_J$ and $W_\eta$ are comparable, a fully coupled steady-state analysis of boundary layers and electrode sheaths would alter the results but not by orders of magnitude. However, the large contribution of $W_J$ to the heat balance could potentially lead to instability. A local increase in temperature and decrease in density would decrease the ionization rate, $\sim T^{-1}$, and electron density, $\sim T^{-1/2}$, but the conductivity would increase proportionally to $\sqrt{T}$. The local Hall parameter would increase, $\sim T$, and so would the Hall current $j_x$. The joule heating rate would then go up as $j_x^2/\sigma \sim \Omega^2/\sigma \sim T^{3/2}$, further increasing the temperature and thus closing the instability loop. A detailed analysis of the onset and dynamics of this instability is possible only with a fully coupled analysis, which is outside the scope of this paper. The anode sheath being quite thin (50–100 $\mu$m), heat conduction would be quite effective in dissipating temperature fluctuations. Also, because insufficient ionization is the primary driving factor for the high joule heating rate, an additional ionization could help to reduce the heating rate and to suppress the instability. The additional ionization can be due to increase in $E_{\text{eff}}/N$ within the region of positive temperature fluctuation, or can be created artificially by manipulating electron beam current. Cases 2 and 3 in Figs. 5 and 6 correspond to increased beam current density in the thin anode sheath: $q = q_{\text{ext}}(N/N_{\text{ext}})^{0.25}$ (case 2) and $q = q_{\text{ext}}(N/N_{\text{ext}})^{0.05}$ (case 3). As seen in Figs. 5 and 6, enhanced ionization indeed reduces $W_J$ to the level below $W_\eta$ (case 3), reducing also sheath thickness, voltage fall, and the electric field.

### D. Effect of Ponderomotive Forces on Boundary Layers

In hot, rarefied boundary layers, ionization kinetics and electrodynamics may be different from those in the core flow. In turn, the body forces existing in MHD channels affect the boundary layers. One important difference between gasdynamics in accelerators and power generators is the sign of the effect of ampere forces on boundary layers. Indeed, whereas in accelerators the ampere force acts along the flow and against viscous friction, accelerating the flow and reducing the boundary-layer thickness (see the preceding discussion), in power generators the $\boldsymbol{j} \times \boldsymbol{B}$ body force is added to the viscous forces, thus making boundary layers thicker. This is shown in Fig. 7, where fluid and thermal boundary-layer profiles are shown at a fixed distance from the constant-area channel inlet and two values of the freestream velocity, for the channel without magnetic field, $B_z = 0$, accelerator, positive $B_z$, and power generator, negative $B_z$. The substantial changes in the boundary layers caused by ampere forces are quite apparent.

### E. Effect of Thermal Ionization in the Boundary Layer

As pointed out in Sec. III, electron beams injected into the channel do very little ionization near the wall. However, hypersonic boundary layers can be very hot, and thermal ionization can be quite substantial there. If the ionization fraction in the boundary layer is much higher than the beam-generated ionization in the core flow, the boundary layer would form a highly conductive channel through which most of the electric current would flow, potentially degrading the channel performance. Note that, in this section, we discuss boundary layers that are not electrode sheaths (left and right layers in Fig. 2).

To estimate the magnitude of this effect, we performed calculations of the turbulent boundary layer in the case of an MHD accelerator with a 20-T magnetic field that reaches Mach 14.5 at $T = 240$ K at the exit. The details of this case are presented in Sec. V. Again, for simplicity we assumed that the ionizing beams, instead of being concentrated in periodic slots, fill out the entire side wall. Taking electric current and core flow density, temperature, and velocity

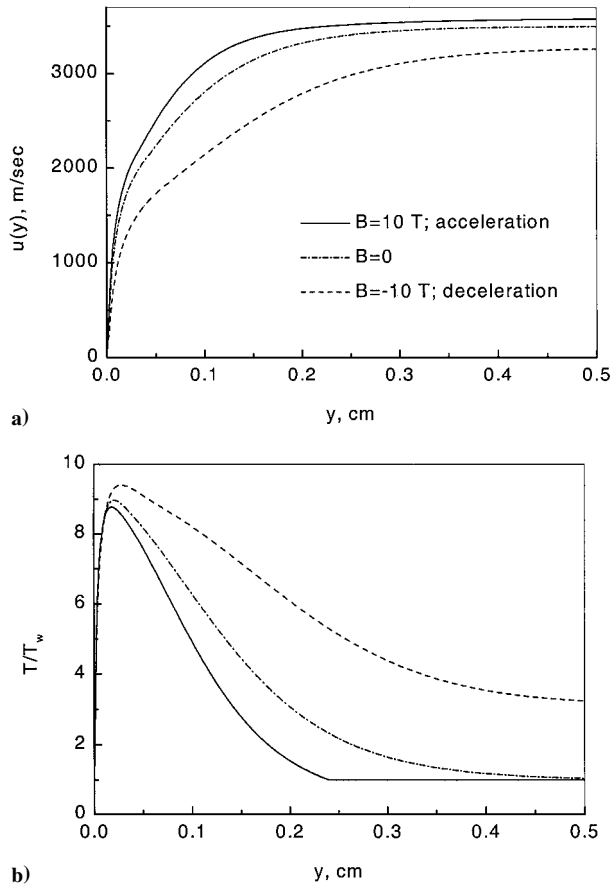


**Fig. 7 Fluid and thermal boundary layer profiles at a fixed location $x = 0.5$ m from the channel inlet; pressure $p = p_0 =$ const; conductivity and transverse electric field assumed uniform along the channel; loading parameter $k = 1.1$. Freestream velocity is $u_0 = 3500$ m/s.**

profiles along the channel from the quasi-one-dimensional calculation of Sec. V, fluid and thermal boundary layers were computed in two limits: an adiabatic wall and an ideally cooled isothermal ($T_w = 300$ K) wall.

The most dangerous situation would occur at the end of the accelerator channel, where gas velocity is the highest. The calculation[12] (with an estimated accuracy of about 5% determined mostly by the accuracy of the equation of state) showed that the peak temperature in the boundary layer is 3700 K for the ideally cooled isothermal ($T_w = 300$ K) wall, but as high as 4500 K in the adiabatic wall case. With the static pressure at this location $p = 0.007$ atm, the thermally equilibrium ionization fractions would be $\alpha_{T=3700\ \mathrm{K}} \approx 5 \times 10^{-6}$ and $\alpha_{T=4500\ \mathrm{K}} \approx 8 \times 10^{-5}$. The electron beam-induced ionization fraction in the core flow at this location is $\alpha_{pl} \approx 4.28 \times 10^{-6}$. Thus, with the peak temperature of 3700 K in the boundary layer, there should be no short circuiting. Even with the 4500-K peak temperature, there seems to be no great danger of short circuiting: Despite the electrical conductivity that is 20 times higher than in the core flow, the highly conductive region is only about 0.3 mm wide, so that the resistance of this layer is equivalent to the resistance of 6-mm-wide slab of core flow air. (The channel width at this location is about 50 cm.)

Other consequences of high electrical conductivity in the boundary layer are related to the potential instability discussed in Sec. IV. C. A fully coupled analysis of this problem is beyond the scope of this paper.

To conclude this subsection, we note that, at Mach numbers of 10 and lower, thermal ionization in the boundary layer of channels with electron-beam ionization would not cause a short circuit. However, at very high Mach numbers, for example, Mach 14, the boundary layer would probably have to be cooled, for example, by injecting a cold gas. Cooling of the boundary layer would have to be done also for other purposes, such as to protect channel walls and foils from erosion and melting.

## V. Quasi-One-Dimensional Modeling of MHD Channels with Electron-Beam Ionization

### A. Basic Equations and Kinetic Rates

To evaluate performance limits of MHD power generators and accelerators with ionization by electron beams, one-dimensional calculations could be very useful. When a specific regime is found promising from the one-dimensional analysis, further two- and three-dimensional computations could be performed to reveal the flow structure: ionization profile, velocity and temperature field, boundary layers, etc. Additionally, in earlier papers,[4,12] we found that two-dimensional modeling with ionization profiles computed with forward or forward–backward approximation gives the same mean flow parameters in any cross section as one-dimensional modeling does. The one-dimensional code should include a reasonably simple but essentially correct model of ionization kinetics and molecular vibrational relaxation.

The latter can certainly be important. Indeed, a substantial portion of the energy that plasma electrons receive from the transverse electric field can be channeled into vibrational excitation of air molecules (primarily, nitrogen). Because the static pressure and temperature in the channels are expected to be low, and the gas residence time inside the channel quite short, most of the energy of vibrational excitation could be simply convected out with the flow, without relaxation. This would affect both gasdynamics inside the channel and the exit flow quality.

When it is assumed that most of the vibrational energy is stored in nitrogen, and nitrogen relaxes in collision with oxygen molecules and atoms, the vibration–translation relaxation time can be written as[21]

$$\tau_{\mathrm{VT}}^{-1} = N\left[7 \times 10^{-10} \exp\left(-141 T^{-\frac{1}{3}}\right) + \alpha_0 \times 5 \times 10^{-12} \exp\left(-128 T^{-\frac{1}{2}}\right)\right], \mathrm{s}^{-1} \tag{19}$$

where $N$ is the total number density of the gas, $T$ is the static temperature in Kelvin, and $\alpha_0$ is the mole fraction of atomic oxygen. The one-dimensional vibrational energy equation then can be written as

$$\frac{\mathrm{d}(N\varepsilon_v)}{\mathrm{d}t} + N\varepsilon_v \nabla \boldsymbol{u} = -\nabla \boldsymbol{q}_v + Q_v - \frac{N\left[\varepsilon_v - \varepsilon_v^0(T)\right]}{\tau_{\mathrm{VT}}(T)} \tag{20}$$

where $q_v$ is the vibrational energy flux due to molecular diffusion. In hypersonic flow, at moderate or high densities, the $q_v$ term is always negligible compared with the convective term. The term $Q_v$ in Eq. (20) is the rate of vibrational excitation per unit volume, and $\varepsilon_v$ and $\varepsilon_v^0(T)$ are the nonequilibrium and thermally equilibrium values of vibrational energy per molecule.

For one-dimensional steady flow, the vibrational energy equation can be rewritten as

$$\frac{\mathrm{d}E_v}{\mathrm{d}x} = \left[Q_v - \frac{E_v - E_v^0(T)}{\tau_{\mathrm{VT}}(T)}\right] \Big/ u + \frac{E_v}{\rho}\frac{\mathrm{d}\rho}{\mathrm{d}x} \tag{21}$$

When the deviation from equilibrium is not very large, nonequilibrium and equilibrium vibrational energy can be expressed through the respective temperatures ($T_v$ is the vibrational temperature) by the Planck formula:

$$E_v = N\varepsilon_v = N\frac{\hbar\omega_0}{\exp(\hbar\omega_0/T_v) - 1}$$

$$E_v^0 = N\varepsilon_v^0 = N\frac{\hbar\omega_0}{\exp(\hbar\omega_0/T) - 1} \tag{22}$$

where $\hbar\omega_0$ is the lowest vibrational quantum of nitrogen molecules. Vibrational free energy and entropy per molecule can be written as

$$\tilde{F}_v = \hbar\omega_0/2 + T_v \ln[1 - \exp(-\hbar\omega_0/T_v)] \tag{23}$$

$$\tilde{S}_v = -k_B\frac{\partial F_v}{\partial T_v} = k_B\left[\frac{\hbar\omega_0}{T_v}\frac{1}{\exp(\hbar\omega_0/T_v) - 1} - \ln[1 - \exp(-\hbar\omega_0/T_v)]\right] \tag{24}$$

Specific, that is, per unit mass, vibrational entropy is $S_v = \tilde{S}_v N/\rho$ J/kg · K.

The vibrational excitation term $Q_v$ can be expressed as a fraction $\eta_v$ of the joule heating rate:

$$Q_v = \eta_v j_y (E_y - uB_z) \tag{25}$$

The fraction $\eta_v \equiv \eta_v((E_y - uB_z)/N) < 1$ is determined on the basis of the solution of Boltzmann kinetic equation for plasma electrons performed and tabulated in Ref. 22.

The vibrational energy equation (21) should be solved together with continuity, momentum, energy, and equation of state equations, assuming an ideal Faraday accelerator:

$$\frac{\mathrm{d}(\rho u A)}{\mathrm{d}x} = 0, \qquad \rho u \frac{\mathrm{d}u}{\mathrm{d}x} + \frac{\mathrm{d}p}{\mathrm{d}x} = j_y B_z$$

$$\rho u \frac{\mathrm{d}(\gamma\varepsilon + u^2/2)}{\mathrm{d}x} = j_y E_y - Q_v + \frac{\left[E_v - E_v^0(T)\right]}{\tau_{VT}(T)} + Q_b$$

$$p = R\rho T = (\gamma - 1)\rho\varepsilon \tag{26}$$

where $A(x) = Z^2(x)$ is the cross-sectional area of the channel, $Q_b = 2j_b\varepsilon_b/eZ$ is the rate of energy addition by the two ionizing electron beams injected from the opposite sides of the channel, $\varepsilon_b$ and $j_b$ are the electron beam energy and current density, and $Z$ is the channel width.

The transverse current density in an ideal Faraday accelerator is

$$j_y = \sigma(E_y - uB_z), \qquad \sigma = e\mu_e n_e \tag{27}$$

where $\sigma$ is the electrical conductivity, $\mu_e$ is the electron mobility, and $n_e$ is the plasma electron number density.

In the case of an ideal Faraday power-generation channel, the set of equations is similar to Eqs. (26) and (27):

$$\frac{\mathrm{d}(\rho u A)}{\mathrm{d}x} = 0, \qquad \rho u \frac{\mathrm{d}u}{\mathrm{d}x} + \frac{\mathrm{d}p}{\mathrm{d}x} = -(1-k)\sigma u B_z^2$$

$$\rho u \frac{\mathrm{d}(\gamma\varepsilon + u^2/2)}{\mathrm{d}x} = -k(1-k)\sigma u^2 B_z^2 - Q_v + \frac{\left[E_v - E_v^0(T)\right]}{\tau_{VT}(T)} + Q_b$$

$$\frac{\mathrm{d}E_v}{\mathrm{d}x} = \left[Q_v - \frac{E_v - E_v^0(T)}{\tau_{VT}(T)}\right] \Big/ u + \frac{E_v}{\rho}\frac{\mathrm{d}\rho}{\mathrm{d}x}$$

$$Q_v = \eta_v(1-k)^2\sigma u^2 B_z^2, \qquad p = R\rho T = (\gamma - 1)\rho\varepsilon \tag{28}$$

where $A = A(x)$ is the MHD channel cross-sectional area.

The loading parameter $k < 1$ for power-generation channels is defined as the ratio of the voltage on the external load in the electric circuit to the electromotive force $uB_z$. Total power extracted from the MHD channel,

$$W_{\mathrm{ext}} = k(1-k)\int_V \sigma u^2 B_z^2 \,\mathrm{d}V$$

and the efficiency, $\chi = W_{\mathrm{ext}}/[\rho u A(u^2/2 + c_p T)]_{x=0}$, can be calculated after solving the gasdynamic equations.

The plasma in both accelerator and power-generator channels is modeled as consisting of electrons and positive and negative ions, whose number densities $n_e$, $n_+$, and $n_-$ obey the quasi neutrality: $n_+ \approx n_e + n_-$. The set of equations for kinetics of charge species, accounting for electron-beam-induced ionization rate ($q_i$ term), attachment of electrons to molecules with formation of negative ions (frequency $\nu_a$), collisional detachment of electrons from negative ions (rate constant $k_d$), and electron–ion and ion–ion recombination (rate coefficients $\beta$ and $\beta_{ii}$, respectively), is

$$\frac{\partial n_e}{\partial t} + \frac{\partial \Gamma_e}{\partial x} = q_i + k_d N n_- - \nu_a n_e - \beta n_+ n_e$$

$$\frac{\partial n_+}{\partial t} + \frac{\partial \Gamma_+}{\partial x} = q_i - \beta_{ii} n_- n_+ - \beta n_+ n_e$$

$$\frac{\partial n_-}{\partial t} + \frac{\partial \Gamma_-}{\partial x} = -k_d N n_- + \nu_a n_e - \beta_{ii} n_- n_+ \tag{29}$$

For one-dimensional stationary flow ($\partial n_{e,+,-}/\partial t = 0$), in the case of $E_x = 0$ (ideal Faraday accelerator or power generator), the fluxes of charged species can be written simply as $\Gamma_{e,+,-}(x) = n_{e,+,-}u$.

The approximation formula for the electron-beam ionization rate is

$$q_i = 2\varepsilon_b j_b/eW_i Z \tag{30}$$

where $W_i$ is the ionization cost (see Sec. III).

Two- and three-body ion–ion recombination in air,

$$A^- + B^+ \Rightarrow A + B, \qquad A^- + B^+ + M \Rightarrow A + B + M \tag{31}$$

can be characterized by the rate coefficient[23]

$$\beta_{ii} = 2\times 10^{-7}(300/T)^{\frac{1}{2}}\left[1 + 1\times 10^{-18} N (300/T)^2\right], \ \mathrm{cm}^3/\mathrm{s}$$

Electron–ion recombination is dissociative:

$$e + \begin{cases} O_2^+ \\ N_2^+ \end{cases} \Rightarrow \begin{cases} O + O \\ N + N \end{cases} \tag{32}$$

with the rate coefficient $\beta = 2\times 10^{-7}(300/T_e)^{1/2}$ (Ref. 23), where $T_e$ is the electron temperature.

The primary processes of three-body electron attachment and their rate coefficients[23]

$$e + O_2 + O_2 \Rightarrow O_2^- + O_2$$

$$k_{a1} = 1.4\times 10^{-29}\left(\frac{300}{T_e}\right)\exp\left(-\frac{600}{T}\right) \times \exp\left(\frac{700(T_e - T)}{T_e T}\right), \ \mathrm{cm}^6/\mathrm{s}$$

$$e + O_2 + N_2 \Rightarrow O_2^- + N_2$$

$$k_{a2} = 1.07\times 10^{-31}\left(\frac{300}{T_e}\right)^2 \exp\left(-\frac{70}{T}\right) \times \exp\left(\frac{1500(T_e - T)}{T_e T}\right), \ \mathrm{cm}^6/\mathrm{s} \tag{33}$$

Because rate coefficients of processes (32) and (33) depend on $T_e$, it is important to calculate the electron temperature in the modeling. In our computations, electron temperature was determined from the tabulated data on electron diffusion and mobility coefficients of Ref. 22. In Ref. 22, the diffusion and mobility coefficients are listed as functions of $E/N$, determined from experimental data and extrapolation based on solution of Boltzmann kinetic equation for electrons in air.

In principle, attachment could also be dissociative:

$$e + O_2 + 3.6\ \mathrm{eV} \Rightarrow O + O^- \tag{34}$$

However, this process has a relatively high threshold, and its rate exponentially depends on $T_e$ or $E/N$. In typical cases of interest for hypersonic MHD channels with electron-beam ionization, the parameter $E/N$, where $E = E_y - uB_z$, is very small, and the process (34) for plasma electrons can be neglected. However, in future work it would be desirable to evaluate the role of process (34) with participation of high-energy beam electrons.

The dominant process of collisional detachment of electrons from negative ions and its rate constant,[24]

$$O_2^- + O_2 \Rightarrow e + 2O_2$$

$$k_{dO_2} = 8.6\times 10^{-10}\exp(-6030/T)[1 - \exp(-1570/T)] \ \mathrm{cm}^3/\mathrm{s} \tag{35}$$

Detachment can also occur in collisions with excited species, for example,

$$O_2^- + O_2\left(a^1\Delta_g\right) \Rightarrow e + 2O_2, \qquad k_{dA} = 2 \times 10^{-10}\ \mathrm{cm^3/s} \quad (36)$$

Detachment in collisions with other active particles has rate coefficients of the same order of magnitude as Eq. (36). Therefore, in general, the frequency of detachment is $\nu_d = k_{dO_2} N_{O_2} + k_{dA} N_A$, where $N_A$ is the number density of active particles. At sufficiently high concentration of active species, electron attachment could be balanced by detachment.

### B. One-Dimensional Modeling of MHD Accelerators with Electron-Beam Ionization

As an example, we computed the case of interest for developing a hypersonic wind tunnel. The tunnel has to generate a flow of air with Mach 12–15 and dynamic pressure of 2000 psf (about 1 atm) continuously (or, at least, with run time of many seconds). The hybrid tunnel[3,4] would consist of three major parts: ultrahigh-pressure plenum, laser or electron beam heating in supersonic expansion, and MHD accelerator.

As a benchmark, we used a case with an ultrahigh-pressure plenum followed by electron beam heating and expansion, without the MHD part. The benchmark case was computed by Robert Anderson of Princeton University using his one-dimensional code that included a real-gas equation of state and a model of energy addition by relativistic electron beams developed by one of the authors (Lipinski). The plenum pressure and temperature were 20,000 atm and 900 K, respectively. The heating by 1–3-MeV electron beams started at Mach 2. The heating and expansion was optimized to add maximum energy to the flow, provided that the static temperature is not allowed to exceed about 2600 K and that the exit temperature, 240 K, and dynamic pressure, 2000 psf, are given. The computation by Anderson estimated that the maximum Mach number achievable under these constraints is about Mach 12.2.

For the hybrid facility (ultrahigh-pressure plenum, heating by relativistic electrons in supersonic expansion, plus MHD accelerator), the energy addition by relativistic electrons was terminated at the point where the gas reaches its maximum temperature. Specifically, for the benchmark case, the static pressure at this point was 206.6 atm, the static temperature 2590 K, and velocity 2829 m/s. The gas then was isentropically expanded to the static pressure of 0.1 atm, at which point its static temperature became 373 K and velocity 3667.6 m/s. These conditions were considered to be the initial conditions at the entrance of the MHD accelerator channel. With mass flow rate of 10 kg/s, the MHD channel is 17 cm wide at the entrance and, with Mach 14.5 at $T = 240$ K at the exit (discussed subsequently), is about 47 cm wide at its exit. The magnetic field in the channel was put at $B = 20$ T.

When the channel performance is optimized, several important constraints have to be obeyed. In addition to the given exit dynamic pressure and static temperature, there are constraints on electric field, loading parameter, and ionizing beam current.

The constraint on the electric field is related to ionization by plasma electrons and a possibility of short circuiting between adjacent electrode segments. Let us consider this problem for a Faraday channel. The key parameter determining ionization processes due to plasma electrons is $E/N$, which is proportional to the energy gained by an electron between collisions. In an ideal Faraday MHD accelerator, the effective electric field is $E = E_y - uB_z$, so that the parameter is $(E_y - uB_z)/N$. If the Hall parameter $\Omega$ in the plasma is large, then in the boundary layer near the segmented electrodes, the electric field is determined mostly by its $x$ component that is designed to eliminate Hall current in the plasma: $E_b = E_x = \Omega(E_y - uB_z)$. However, because electrons in the boundary layer have to move across the strong magnetic field at high Hall parameters, their effective mean free path is determined by spiraling around magnetic field lines rather than by collisions. Because the Larmor radius is proportional to magnetic field and does not depend on density, it is the product $N_b \cdot \Omega_b$ (subscript $b$ denotes boundary layer) that should be used instead of just $N_b$ to determine the $E/N$ parameter in the boundary-layer near electrodes. However, because Hall parameter is inversely proportional to density, the ratio $E_b/(N_b \cdot \Omega_b)$ is equal to $(E_y - uB_z)/N$. Thus, it is the parameter $(E_y - uB_z)/N$ that defines the intensity of ionization processes induced by plasma electrons both in the core flow and near electrodes.

To avoid electric breakdown between the electrode segments, the $(E_y - uB_z)/N$ parameter should be kept low: $(E_y - uB_z)/N \ll 100$ Townsend (Td), where 1 Td $= 10^{-17}$ V $\cdot$ cm$^2$. However, there is a more restrictive condition imposed on $(E_y - uB_z)/N$: For stability, the plasma has to be non-self-sustained and fully controlled by electron beams, so that the rate of ionization by plasma electrons has to be less than that by the beams. This condition can be approximately expressed as $(E_y - uB_z)/N <$ 20 Td.

For the best performance, push work in the accelerator should be maximized, while joule heating that results in entropy increase should be minimized. Therefore, the loading parameter, $k = E_y/(uB_z)$, should be kept very close to 1. This makes the electric current and the $\boldsymbol{j} \times \boldsymbol{B}$ force small, so that a longer channel is required to provide the necessary kinetic energy augmentation. Also, with $k$ close to 1, gas velocity quickly reaches the limit $E_y/B_z$. With the uniform and constant magnetic field, further acceleration would require an increase in the transverse electric field. However, from the Maxwell equation (17), it is clear that $E_x$ does not vary with $y$ only when the transverse field $E_y$ is constant along the flow. The longitudinal field $E_x = \Omega(E_y - uB_z)$, created by independently biasing electrode segments, is necessary to eliminate Hall current. Therefore, if the transverse electric field varies along the channel, the complete elimination of the Hall current becomes impossible, and the channel performance will deteriorate.

A solution to the problem of maximizing performance while keeping $E_y$ constant along the channel is to have several consecutive MHD channels, each with its own $E_y$. At the end of the first channel, the flow would reach its maximum velocity $E_y/B_z$. Then, the flow would enter the second channel, with slightly higher $E_y$, reach the new maximum velocity, etc. If the loading parameter $k$ is very close to 1, the channel length may become shorter than its width,

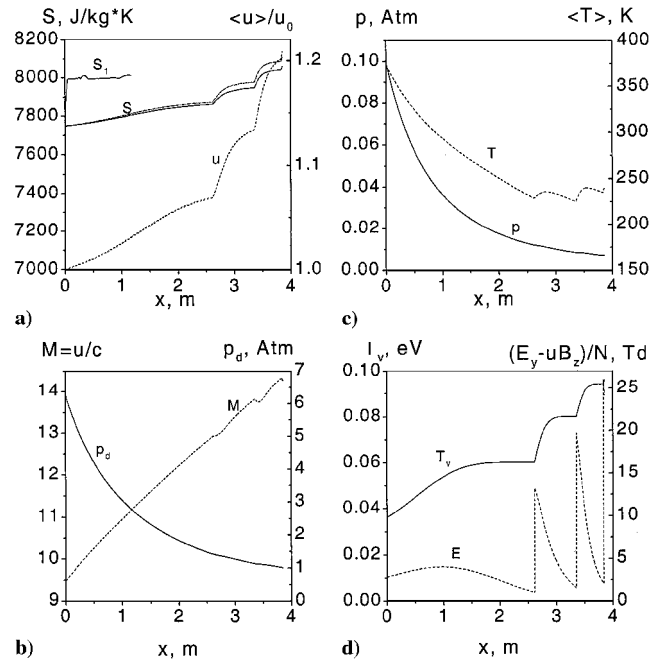


**Fig. 8 Computed profiles of gas parameters along the channel in the MHD accelerator case with electron beam injection through periodic slots: a) $S_1$ is specific entropy variation for the case with energy addition by a relativistic electron beams with no MHD, $S$ is specific entropy variation for the MHD case (solid line is translational–rotational entropy and dashed line full entropy, including vibrational entropy), $\langle u \rangle/u_0$ is gas velocity averaged over the channel cross section, $\langle u \rangle$, relative to the initial velocity $u_0$; b) profiles of dynamic pressure $p_d$ and the Mach number $M$; c) temperature and pressure variation along the channel ($\langle \cdots \rangle$ means averaging over the channel cross section); and d) vibrational temperature $T_v$ and the effective electric field strength variation along the channel.**

which would lead to a nonuniform electric field, again reducing the channel performance. Therefore, $k$ should not be too close to 1: $l_s \ll a(x)$ for $E_y$ uniformity.

Another important parameter is the current density of the ionizing electron beams. This current density should be kept low, about 1 mA/cm$^2$, to minimize heating and entropy increase in the MHD channel. This relatively low beam current density also alleviates beam injection and foil heating problems. However, the resulting electrical conductivity in the channel is not high. To compensate for the reduced conductivity, very strong magnetic fields and very long channels may be needed.

The set of Eqs. (26) [or Eqs. (28), in the generator case in Sec. V. C] and (29) at steady state was solved by the modified second-order Euler method. The number of equal spatial steps was $n \geq 1000$. Further increasing the number of steps was found to produce negligible variation of results.

Figures 8 and 9 show the computed results for the periodic-slot electron beam injection. The width of each slot was 0.5 cm, with 2-cm spacing between the slots. The current density of electron beams was $j_b = 3.5$ mA/cm$^2$ and the magnetic field strength 20 T. The best results were obtained with the loading parameter of 1.075 in the first subchannel and 1.06 in subsequent subchannels. The

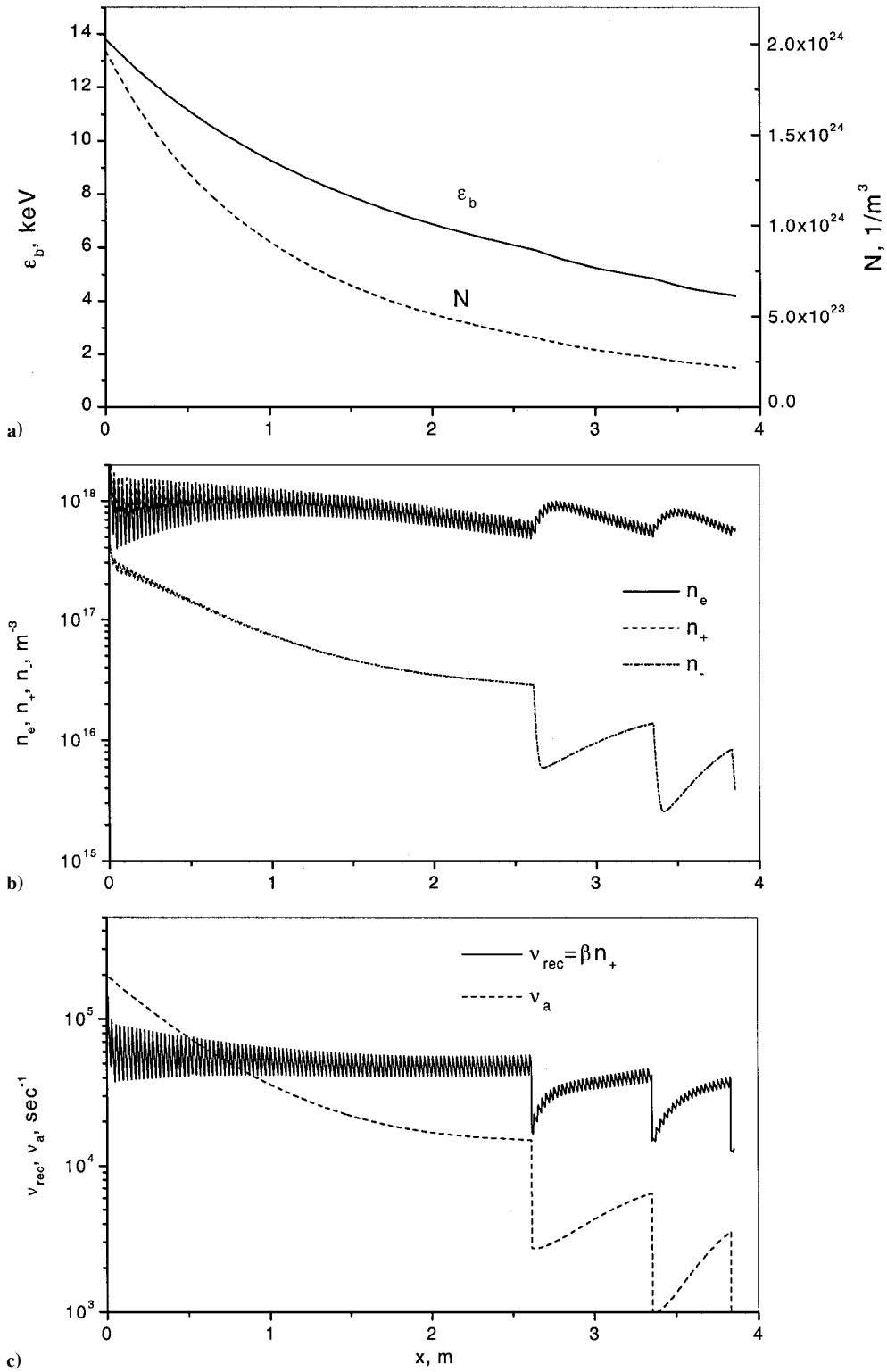


**Fig. 9 Profiles of electron beam energy $\varepsilon_b$, gas number density $N$, number densities of electrons and positive and negative ions $n_e$, $n_i$, and $n_n$, and electron recombination and attachment frequencies $\nu_{rec}$ and $\nu_a$ for the case shown in Fig. 8.**

boundaries between the subchannels are clearly seen in Fig. 8d as points where electric field strength experiences sharp jumps. Because of the sensitivity of recombination and attachment rates to electron temperature, which in turn depends on electric field, sharp jumps are also seen in the corresponding curves in Figs. 9b and 9c.

As seen in Fig. 8, this configuration generates Mach 14.3 at 2000 psf, with the channel length of 3.8 m. Figures 9b and 9c show profiles of charged-particle densities and electron removal rates along the channel. The oscillations of number densities of electrons and positive ions and of recombination rate are a result of ionizing electron beams being injected through periodically spaced slots (see Fig. 1); between the slots, plasma only decays. With the proper spacing between the slots, the number densities of electrons and positive ions stay close to $10^{12}$ cm$^{-3}$, with relatively little variation. Because of the decreasing gas density, electron attachment plays a role only in the first meter of the channel. In the rest of the channel, it is electron–ion dissociative recombination that determines electron balance.

As seen in Fig. 8d, vibrational temperature reaches almost 0.1 eV at the exit. Although this constitutes only a very small fraction of the total enthalpy, the vibrational-translational nonequilibrium is quite pronounced. To check how sensitive this result is to air chemistry that was not coupled with the gasdynamics, we computed the variation of characteristic vibrational relaxation time along the channel at different mole fractions of atomic oxygen.[12] Because the residence time of molecules inside the channel is less than a millisecond, only a very large mole fraction of atomic oxygen, on the order of 10%, could affect the relaxation. Because such mole fractions could hardly be expected to exist in the channel, removal of vibrationally excited molecules would proceed primarily by convection with the hypersonic flow. Because nitrogen vibrational relaxation rate in collision with water molecules is comparable with that in collisions with oxygen atoms, it is also unlikely that a presence of water vapor would affect vibrational kinetics under these conditions.

The computations were performed assuming an ideal quasi-one-dimensional Faraday channel. However, such an ideal channel may be difficult to realize. Because of the high Hall parameters in the core flow, and even higher boundary-layer Hall parameters, electric current in the boundary layer near the anode would flow at a grazing angle with respect to the anode. This could lead to current concentration at the edges of anode segments and arcing between the segments. Ways to minimize such undesirable effects and more sophisticated three-dimensional models that would take into account Hall currents in the boundary layer should be considered in future.

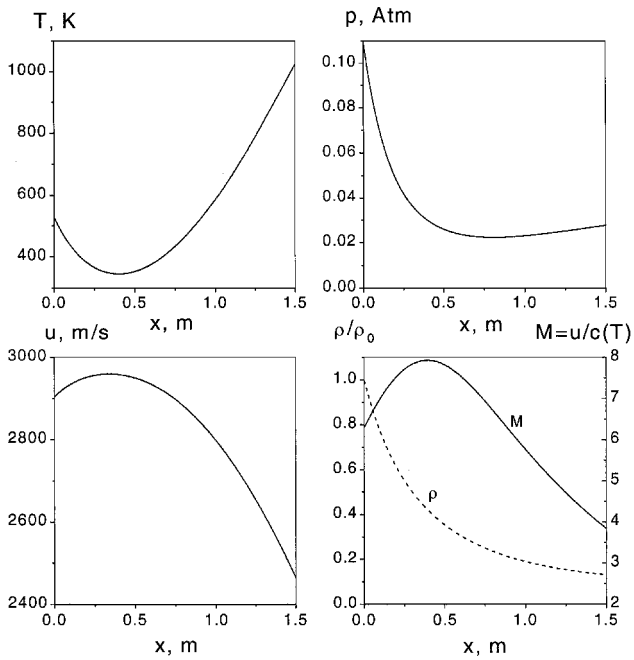


**Fig. 10 Profiles of temperature, pressure, velocity, density, and Mach number in the MHD power generator case.**

Another consequence of operation at high Hall parameters is that the so-called ion slip[19] could play a role, somewhat (not dramatically) reducing performance of the MHD device.[25] Again, a detailed analysis of this effect should be a subject of further work.

### C. One-Dimensional Modeling of Hypersonic MHD Power Generators with Electron-Beam Ionization

One-dimensional modeling of MHD power generators is similar to that of accelerators, as detailed in Sec. V.A. The constraints are also similar to those imposed in Sec. V.B. The performance requirements that we imposed in calculations are to maximize the extracted power while keeping the static temperature within about 1000 K. The example case corresponds to Mach 10 flight at 97,000-ft altitude, where the static temperature is about 240 K and the static pressure is $1.54 \times 10^{-2}$ atm. A 10-deg wedge was assumed to create a shock upstream of the MHD channel. The flow parameters behind the shock are $p = 0.10915$ atm, $T = 528$ K, $u = 2903.7$ m/s, and $M = 6.34$.

The channel geometry was that shown in Fig. 1, with the entrance cross section of $15 \times 15$ cm, exit cross section of $45 \times 45$ cm, and a length of 1.5 m. A magnetic field of 7 T, representing the current practical limit of superconducting magnets, was used in the calculations. As in the accelerator case, ionizing electron beams were assumed to be injected through windows forming an array of periodic slots, each slot being 0.5 cm wide, with 2-cm spacing between the slots.

Figures 10 and 11 show the results for Mach 10 at 97,000-ft altitude and shock produced by a 10-deg wedge upstream of the channel entrance. The entrance cross section $A_{in} = 0.15 \times 0.15$ m$^2$ and exit cross section $A_{out} = 0.45 \times 0.45$ m$^2$. The magnetic field $B = 7$ T. Electron beams are injected from both sides through periodic 0.5-cm-wide slots spaced by 2 cm. Note that in a similar case with flight Mach number of 5, computed in Ref. 12, Mach 1 at a static temperature of 864 K was obtained at the MHD channel exit. The extracted power constituted 22.6% of the total enthalpy flux into the channel, translating into 524 kW. In the present Mach 10 case, bringing flow to sonic while keeping the static temperature below 1000 K

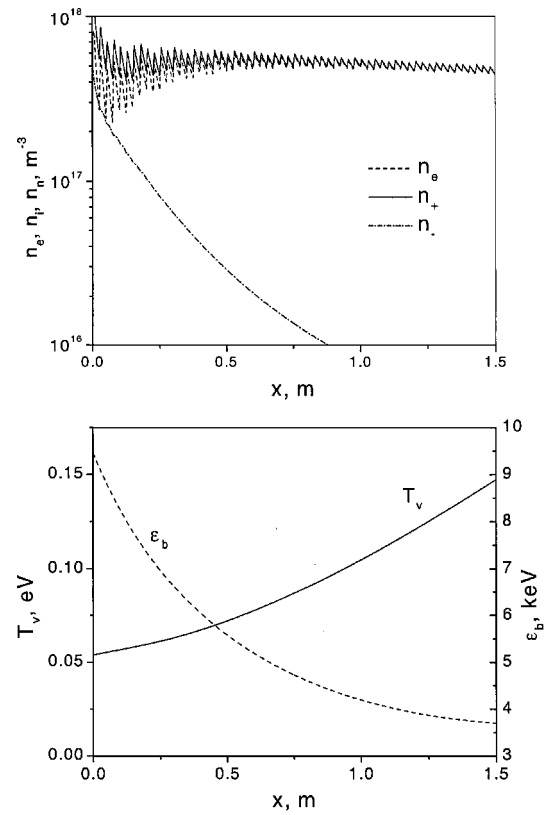


**Fig. 11 Profiles of charged particle densities, vibrational temperature, and electron-beam energy for the Mach 10 MHD generator case shown in Fig. 10.**

turns out to be very difficult if not impossible. In the computations, we were able to get down to Mach 3.7 at about 1000-K static temperature. The electron-beam current density $j_b = 1$ mA/cm$^2$ and the loading parameter $k = 0.82$. The extracted power constitutes 13.8% of the total enthalpy flux into the channel, translating nevertheless into an impressive $W_{\text{output}} = 2.95$ MW. The power input by the ionizing beams is only 8.72 kW.

The electron-beam power requirements are important because that power would come from the electricity generated in the channel. The actual power requirements are higher than the 8.72 kW of power brought by the beams into the channel in the two cases. Perhaps the most important additional power requirement is dictated by the need for the beams to pass through windows. Energy loss in a typical foil is about 30–50 keV. The total foil area in both cases is about $2 \times 900 = 1800$ cm$^2$, and the beam current density is 0.8–1 mA/cm$^2$. Therefore, the beam power losses can be estimated as 90 kW or less. Even with these losses, the total beam power requirements are still substantially less than the extracted electric power.

## VI. Summary

We analyzed and developed a novel concept of cold-air hypersonic MHD power generators and accelerators, based on ionization by electron beams. Special attention was paid to such issues as ionization kinetics, uniformity of beam-generated ionization profiles, and the important role of boundary layers and electrode sheaths. The analysis demonstrated that, with careful choice of parameters, electron beams could form stable, well-controlled plasmas, avoiding many shortcomings of conventional MHD channels and potentially enabling an impressive level of performance for both generators and accelerators.

A number of critical technical and engineering issues would have to be resolved to make hypersonic MHD channels practical. At this time, two groups of issues appear to be the most important. The first is cooling of the walls, electrodes, electron-beam pass-through windows, and the boundary layer. Further theoretical work should include taking into account ion slip effects and Hall current in the near-anode boundary layer and developing three-dimensional models. Stability issues, including anode-sheath instabilities and inter-electrode arcing, should be addressed in future work. The second group of issues is developing a control system, including monitoring key parameters of the channel and controlling electron-beam parameters and voltages on multiple electrode segments.

Experimental studies of MHD channels with ionization by electron beams and validation of the models against the experiments would be quite valuable.

## Acknowledgments

This work was supported by MSE, Inc., as a part of the U.S. Air Force MARIAH II Program and by the National Science Foundation.

## References

[1]Fraishtadt, V. L., Kuranov, A. L., and Sheikin, E. G., "Use of MHD Systems in Hypersonic Aircraft," *Technical Physics*, Vol. 43, No. 11, 1998, pp. 1309–1313.

[2]Gurijanov, E. P., and Harsha, P. T., "AJAX: New Directions in Hypersonic Technology," AIAA Paper 96-4609, 1996.

[3]Macheret, S. O., Miles, R. B., and Nelson, G. L., "Feasibility Study of a Hybrid MHD/Radiatively Driven Facility for Hypersonic Ground Testing," AIAA Paper 97-2429, 1997.

[4]Macheret, S. O., Shneider, M. N., Miles, R. B., Lipinski, R. J., and Nelson, G. L., "MHD Acceleration of Supersonic Airflows Using Electron Beam Enhanced Conductivity," AIAA Paper 98-2922, 1998.

[5]Bychkov, Y. I., Korolev, Y. D., and Mesyats, G. A. *Injection Gaseous Electronics (Inzhektsionnaia Gazovaia Elektronika)*, Nauka, Moscow, 1982, Chap. 2 (in Russian).

[6]Hershcovitch, A., "A Plasma Window for Vacuum-Atmosphere Interface and Focusing Lens of Sources for Nonvacuum Ion Material Modification," *Review of Scientific Instruments*, Vol. 69, No. 2, 1998, pp. 868–873.

[7]Hershcovitch, A., "A Plasma Window for Transmission of Particle Beams and Radiation From Vacuum to Atmosphere for Various Applications," *Physics of Plasmas*, Vol. 5, No. 5, 1998, pp. 2130–2136.

[8]Berger, M. J., and Seltzer, S. M., "Tables of Energy Losses and Ranges of Electrons and Positrons," NASA SP-3012, 1964.

[9]Halbleib, J. A., Kensek, R. P., and Valdez, G. D., "ITS: The Integrated TIGER Series of Electron Photon Transport Codes: Version 3.0," *IEEE Transactions on Nuclear Science*, Vol. 39, No. 4, 1992, pp. 1025–1030.

[10]Raizer, Y. P., and Shneider, M. N., "Simplified Kinetic Equation for Electrons in Nonuniform Fields of Arbitrary Strength in Connection with the Cathode Sheath of a Glow Discharge," *Soviet Journal of Plasma Physics*, Vol. 15, No. 3, 1989, pp. 184–189.

[11]DiCarlo, J. V., and Kushner, M. J., "Solving the Spatially Dependent Boltzmann's Equation for the Electron Velocity Distribution Using Flux-Corrected Transport," *Journal of Applied Physics*, Vol. 66, No. 12, 1989, pp. 5763–5774.

[12]Macheret, S. O., Shneider, M. N., and Miles, R. B., "Electron Beam Generated Plasmas in Hypersonic MHD Channels," AIAA Paper 99-3635, 1999.

[13]Shneider, M. N., Macheret, S. O., and Miles, R. B., "Electrode Sheaths and Boundary Layers in Hypersonic MHD Channels," AIAA Paper 99-3532, 1999.

[14]Cebeci, T., and Smith, A. M. O., *Analysis of Turbulent Boundary Layers*, Academic Press, New York, 1974, Chaps. 5, 6, and 9.

[15]Anderson, D. A., Tannehill, J. C., and Pletcher, R., *Computational Fluid Mechanics and Heat Transfer*, Hemisphere, New York, 1984, Chap. 5.

[16]Raizer, Y. P., *Gas Discharge Physics*, Springer, Berlin, 1991, Chap. 14.

[17]Golant, V. E., Zhilinsky, A. P., and Sakharov, I. E., *Fundamentals of Plasma Physics*, Wiley, New York, 1980, Chap. 5.

[18]Jahn, R. G., *Physics of Electric Propulsion*, McGraw–Hill, New York, 1968, Chap. 8.

[19]Rosa, R. J., *Magnetohydrodynamic Energy Conversion*, McGraw–Hill, New York, 1968, Chap. 3, 4.

[20]Kerrebrock, J. L., "Electrode Boundary Layers in Direct-Current Plasma Accelerators," *Journal of the Aerospace Sciences*, Aug. 1961, pp. 631–644.

[21]Macheret, S. O., Martinelli, L., and Miles, R. B., "Shock Wave Propagation and Structure in Non-Uniform Gases and Plasmas," AIAA Paper 99-0598, 1999.

[22]Aleksandrov, N. L., Vysikailo, F. I., Islamov, R. Sh., Kochetov, I. V., Napartovich, A. P., and Pevgov, V. G., "Electron Distribution Function in 4 : 1 $N_2$–$O_2$ Mixture," *High Temperature*, Vol. 19, No. 1, 1981, pp. 17–21.

[23]Kossyi, I. A., Kostinsky, A. Y., Matveyev, A. A., and Silakov, V. P., "Kinetic Scheme of the Non-Equilibrium Discharge in Nitrogen–Oxygen Mixtures," *Plasma Sources Science and Technology*, Vol. 1, No. 3, 1992, pp. 207–220.

[24]Bazelyan, E. M., and Raizer, Y. P., *Spark Discharge*, CRC Press, Boca Raton, FL, 1997, Chap. 2.

[25]Macheret, S. O., Shneider, M. N., and Miles, R. B., "MHD Power Extraction from Cold Hypersonic Air Flow with External Ionizers," AIAA Paper 99-4800, Nov. 1999.

P. Givi
*Associate Editor*